Application of Conditional Random Fields to Pixel-Level Salient Object Detection Through Local, Regional and Global Features

Jimmy Lin
Australian National University
Canberra, Australia
linxin@gmail.com

Christopher Claoué-Long
Australian National University
Canberra, Australia
u5183532@anu.edu.au

Abstract

Making use of OpenCV, DARWIN and the MSRA dataset, we detect the saliency of an object in an image by extracting local, regional and global features at the pixel level, combined with pre-fitted weights derived via logistic regression. A conditional random field is then constructed to capture the spatial continuity of the salient object, with a weighting ratio of combined unary and pairwise terms determined through cross-validation. The binary mask inferred by the conditional random field is then used to output a single bounding rectangle around a salient area through a winner-takes-all algorithm to label the detected salient object, by which the performance of our approach is evaluated through mean boundary displacement error.

1. Introduction and Motivation

A long-standing problem in the field of computer vision is how to calculate the saliency of objects in an image, that is, their prominence in the image when compared to their background and surrounds. Human vision can accomplish this quite easily, since the human brain has mechanisms to direct attention to the main objects in the perceived image. This ability has been studied by researchers in multiple fields, from physiology and psychology, to computer science. The property of detecting a salient object is important for the latter because it leads to the ability to single out individual areas of an image, for example in automatic image cropping and vision simulation in robotics, as well as 3D surface reconstruction in augmented reality displays. Salient object detection is still a field of active research, with multiple avenues being currently pursued.

2. Related Works

Most existing approaches are based on a bottom-up computational framework, where the computer's simulation of visual attention is driven by low-level stimuli in the scene

Figure 1. Example images from MSRA dataset B

[4][5][8]. These approaches employ three steps, the first of which is feature extraction. Multiple low-level visual features such as intensity, colour, orientation, texture, and motion are extracted from the image at multiple scales and are then incorporated into a framework to aid in the detection of the salient object.

The second step is saliency computation. The saliency is computed by a centre-surround operation, self-information, or graph-based random walk using multiple features. After normalisation and linear/nonlinear combination, a master or saliency map is computed to represent the saliency of each pixel in the image.

Finally, a few key locations on the saliency map are identified by winner-take-all, inhibition-of-return, or other nonlinear operations and output as a label designating the salient area in the image.

3. Our Approach

In our approach, we use the open source DARWIN machine learning framework [3] as the basis for our code. We employ the MSRA dataset as the base images for our salient object detection, and build an algorithm from several suppo-

sitions that relate to how human vision differentiates salient objects from the rest of the perceived field of view. People naturally pay more attention to salient objects in images, such as a person, a face, a car, an animal, or a road sign (Figure 1). This attention can be mimicked in computer vision through several factors, which were brought forward by Liu et. al in their research [6][7].

First of all, it is likely that pixels with a high contrast difference to their near neighbours to be part of a salient object, since they could represent a contour or boundary around an object. This is similar to how the human brain discovers boundaries between objects in its visual field by detecting differences in light intensity.

Salient objects are more often than not quite distinct from their local surrounding region. Calculating the difference between an object and its surrounds can therefore give us information about how salient that object is. If we apply this concept over the entire image, we can gather information about how different various areas are to their surrounds to work out the likelihood that those areas are salient.

Finally, humans perceive object prominence through how distinctly coloured they are compared to the rest of the visual field. Indeed, salient objects often demonstrate a marked difference in colour to the rest of a scene. Therefore, the more widely distributed a colour is in an image, the less likely it is that the salient object will contain that colour. The global colour distribution in an image can therefore be used to describe the saliency of the pixels contained within.

3.1. Formulation

To turn the problem of salient object detection into a mathematical formulation, we incorporate these three high-level concepts into the process of creating a saliency map. Salient object detection can be thus formulated as a binary labelling task that separates a salient object from the background through multiple operations.

For each pixel x of given an image I, the binary mask A_x must indicate whether it belongs to the salient object (1) or not (0). Our objective is to compute this mask A in order to show the location of the salient object in the image.

To do this, we build up a probabilistic model

$$P(A|I) = \frac{1}{Z}e^{-E(A|I)}$$

to determine the probability of a binary mask over an image with $\frac{1}{Z}$ as the normalising factor, and $E(A|I)$ as an energy function incorporating both unary and pairwise potentials between pixels in the image

Formally, the energy function can be represented as

$$E(A|I) = \sum_{x} S_{unary}(a_x, I) + \lambda_0 \sum_{x,x'} S_{pair}(a_x, a_{x'}, I)$$

where λ_0 is the relative weight between the sum of multiple unary and pairwise features.
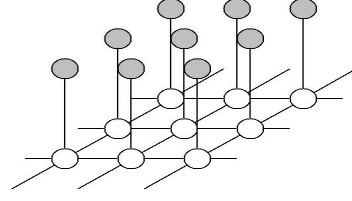

Figure 2. A Conditional Random Field
White nodes are binary saliencies, grey nodes are composite pixelwise features

The unary potential, combining the three pixel features, is specified as

$$S_{unary}(a_x, I) = \sum_{k=1}^{K} \lambda_k \cdot F_k(a_x, I)$$

where λ_k is the weight of the kth feature.

The pairwise feature $S(a_x, a_{x'}, I)$ exploits the spatial relationship between two adjacent pixels. It can be viewed as a "penalty" for labelling adjacent pixels differently:

$$S(a_x, a_{x'}, I) = |a_x - a_{x'}| \cdot e^{-\beta \cdot d_{x,x'}}$$

where x, x' represent two adjacent pixels, $d_{x,x'}$ is the L2-norm (standard norm) representing the colour difference between the two pixels, and $\beta = (2\langle ||I_x - I_{x'}||^2 \rangle)^{-1}$ is a robust parameter to weight the colour contrast.

The final energy map $F_k(a_x, I)$ is calculated from the normalised feature map $f_k(x, I) \in [0, 1]$, where for each pixel:

$$F_k(a_x, I) = \begin{cases} f_k(x, I), & a_x = 0 \\ 1 - f_k(x, I), & a_x = 1 \end{cases}$$

Each pixel is given a penalty if its feature map value $f_k(x, I)$ shows it is not predicted to be within the salient object ($a_x = 0$).

3.2. Feature Extraction

Feature Extraction, widely acknowledged as the most significant component of a computer vision task, represents
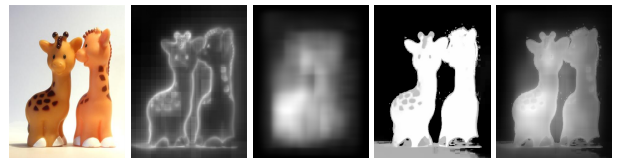

Figure 3. Original Image and Preview of feature maps

Left to Right: Original Image, Multiscale Contrast Map, Centre-Surround Histogram, Colour Spatial Distribution, Composed Unary Potentials

how we want the computer to interpret raw images. In this project, we focus on three features capable of capturing saliency individually but in different levels of scope. They are respectively multiscale contrast, centre-surround histograms and colour-spatial distribution.

Because of the time expense required to calculate these features on an image, our approach caches the feature maps of each image and uses them for both training and testing.

3.2.1 Multiscale Contrast

Constrast is commonly used as local feature because it simulates the human visual receptive fields. It acts on the fact that the boundary of salient objects tend to have a marked contrast to the surrounding region. Since we may have no prior knowledge about the size of salient object, we compute the contrast at multiple scales to then incorporate back into one map, since this will demarcate the various boundaries in the image. This multiscale contrast map is thus a linear combination of image contrast at all levels of an N-level gaussian image pyramid, using the pixels x in the image I. Formally, this amounts to calculating

$$ f_c(x, I) = \sum_{n=1}^{N} \sum_{x' \in W(x)} ||I^n(x) - I^n(x')||^2 $$

where W(x) is a window that delineates which area to consider as neighbouring pixels to compare contrast values. The resulting map highlights the edges of different objects in the image, giving high prominence to the contours around the salient object.

In our implementation, we choose the total number of pyramid level N to be 6 and the size of the window W to be 9×9.
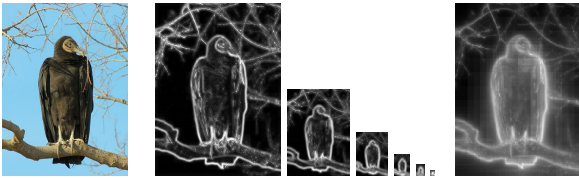
Figure 4. Multiscale Contrast.
Left: Original Image. Right: Multiscale Feature Map.
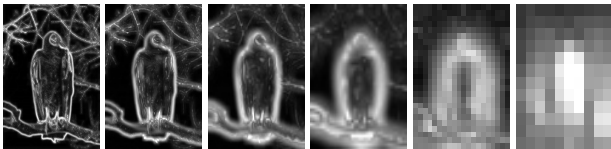Middle: multiscale image pyramid from level 1 to 6.

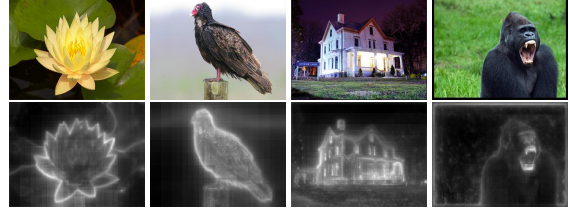Figure 5. Scaled Pyramid Images from level 1 to 6.

Figure 6. Multiscale Contrast Feature Maps

As can be seen in Figure 4, the derived multiscale contrast map provides a highly accurate distinction between boundary and non-boundary pixels. This provides us a precise description of where the boundary of a salient object should exist in the output binary mask. When a salient object also has high contrast inside its boundaries, this feature also manages to capture the inside of the salient object, such as the house and bird in Figure 6.

However, there are some drawbacks that are hard to avoid. Salient objects are not just detected by their boundaries, since doing so would give a high probability to all edges regardless of whether they belong to the salient object or not. This can result in a "saliency leak" into other areas of the image that could deteriorate the detector's precision.

Another disadvantage to only using multiscale contrast is that the inner regions of salient objects are poorly represented. For example in the gorilla in Figure 6, the teeth are labelled as higher contrast to their surroundings compared to that of the body of the gorilla to the grass. Since each entry of the output feature map is quantitatively normalised, the contrast of the gorilla's body to the grass is rendered trivial compared to the contrast of the tooth. The tooth is not what the human receptive field would label as salient because it is a smaller part of the animal, and thus it should not be labelled as the salient object. This flaw may result in low recall comparing to the ground truth data when contrast is used as the sole method to distinguish a salient object.

3.2.2 Centre-Surround Histogram

Multiscale contrast only partially detects salient objects, since it is only sensitive to the boundaries. In order to detect the object as a whole, we make use of another static salient feature which captures the regional information of an area, computed using various low-level features in a centre-surround distance calculation.

To do this, we create a colour RGB histogram for both the rectangle and a surrounding frame with the same area, at a certain resolution (number of "bins" in the histogram). We then measure the difference between the area centred at each pixel x and its surrounds by calculating the chi-

squared distance between the two histograms representative of those regions. We do this for multiple aspect ratios $\{0.5, 0.75, 1.0, 1.25, 1.5\}$, and keep the largest (most distinct) chi-squared value through the formula

$$R(x) = \arg\max_{R(x)} \chi^2(R(x), R_s(x))$$

$$= \arg\max_{R(x)} \frac{1}{2} \cdot \sum_{i \in bins} \frac{(hist_{R(x)_i} - hist_{R_s(x)_i})^2}{hist_{R(x)_i} + hist_{R_s(x)_i}}$$

To reduce the computational complexity involved in this calculation, the size of the rectangle bounding the area in the centre is reduced to 12 discrete ratios $\{0.18, 0.2, 0.25, 0.3, 0.35, 0.4, 0.45, 0.5, 0.55, 0.6, 0.65, 0.7, 0.75\}$ with regards to $min(w, h)$, the minimal value of width and height of the processed image.

The centre-surround histogram feature map at each pixel x is calculated by

$$f_h(x, I) \propto \sum_{x'|x \in R(x')} w_{xx'} \chi^2(R(x'), R_s(x'))$$

where $w_{xx'}$ is a falloff weight which reflects how distinct each pixel is from its surrounds, assigned from the largest χ^2 value for the area centred at each pixel of the image and its surrounds, and its distance from the centre of that area.

As shown in Figure 7, the salient block within the image is given significant emphasis in the output feature map when compared to its surrounds. However, unlike multiscale contrast, the centre-surround histogram does not provide an accurate description of the boundary of the object Used together with the multiscale contrast map, the two features complement the weaknesses to create a stronger sense of the location of salient objects.

3.2.3 Colour Spatial Distribution

The goal of using colour spatial distribution is to take into account the global colour information in the image, that is, the information about how widely the colours that occur in one image are distributed within it. The computation of this feature is done in several parts.
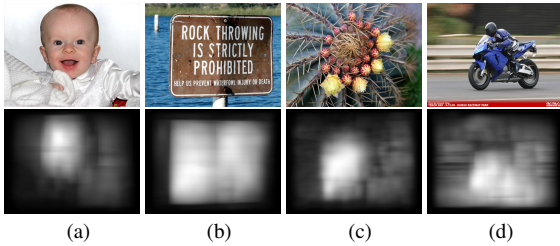

(a)   (b)   (c)   (d)

Figure 7. Centre-Surround Histogram Feature Maps

(a)   (b)   (c)   (d)
(a) Original (b) No reduction (c) Single Level Reduction
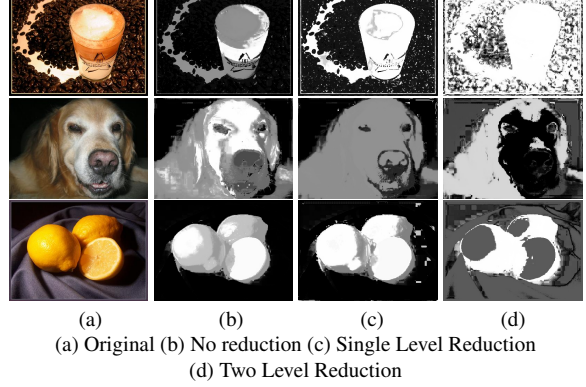(d) Two Level Reduction
Figure 8. Example Colour Spatial Distributions on Reduced Pixels

First of all, we create a Gaussian mixture model with 5 components in order to capture relative colour distribution in the image. This can be represented as $\{c, \mu_c, \Sigma_c\}$ with regards to the colour component c and fit of these components, the mean colour and the covariance of the component c. We use only a subset of pixels from the whole image to save on computational time required to process the feature, while at the same time not losing much accuracy as can be seen in Figure 8. We test three levels of pixel reduction via a Gaussian image pyramid: none, single-level reduction, and two-level reduction. Single-level reduction halves the number of pixels used in creating the gaussian mixture model, whilst also providing a smoother distribution without sacrificing required accuracy. The maximum number of iterations over the image is limited to 100 instances, and the convergence criterion is also lowered to 10^{-1} in order to reduce complexity without deteriorating the model. Such simplification is possible only because the exact distribution is not required for capturing the approximate location of a salient object.

Using this model, each pixel is associated to a colour component with the probability

$$P(c|I_x) = \frac{\omega_c \mathcal{N}(I_x|\mu_c, \Sigma_c)}{\sum_c \omega_c \mathcal{N}(I_x|\mu_c, \Sigma_c)}$$

where ω_c is the weight, μ_c is the mean colour, Σ_c is the covariance, and $\mathcal{N}(I_x|\mu_c, \Sigma_c)$ is the multivariate normal distribution of the cth component.

For each fitted colour component c, we compute its horizontal variance $V_h(c)$ by

$$V_h(c) = \frac{1}{|X|_c} \sum_x p(c|I_x) \cdot |x_h - M_h(c)|^2$$

where x_h is horizontal coordinate of pixel x, $|X|_c$ is normalising factor and $M_h(c)$ is the mean of the gaussian com-
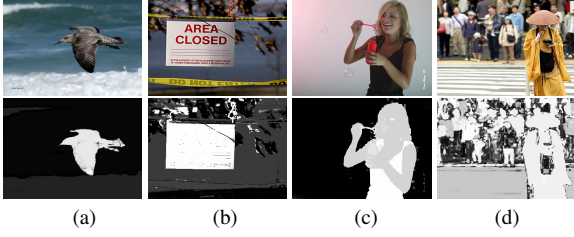
Figure 9. Colour Spatial Distribution Feature Maps

ponent

$$|X|_c = \sum_x p(c|I_x) M_h(c) = \frac{1}{|X|_c} \sum_x p(c|I_x) \cdot x_h$$

Its vertical variance $V_v(c)$ is defined similarly, and we combine the horizontal and vertical variances to derive the unnormalised composite variance $V'(c)$:

$$V'(c) = V_h(c) + V_v(c)$$

We then employ a min-max approach to normalise the composite covariance over the image

$$V(c) = \frac{V'(c) - min(V'(c))}{max(V'(c)) - min(V'(c))}$$

where $V(c)$ is the normalised composite covariance of the cth component, contained between 0 and 1.

Finally, due to the supposition that a salient object tends to have a less widely distributed colour, we set a penalty on the pixels which have a high variance colour. The ultimate colour spatial distribution feature for pixel x is therefore defined as a weighted sum of its colour distribution

$$f_s(x, I) \propto \sum_c p(c|I_x) \cdot (1 - V(c))$$

The final feature map $f_s(x, I)$ is normalised to fall between $[0, 1]$. Figure 9 demonstrates the colour spatial distribution feature map on several images. The salient objects are labelled effectively by this global feature when there is a high distribution of other colours in the image.

It is evident that this global feature allows the detector to find salient objects with much greater accuracy when the background is monotonous. However, in the case of a varied and colourful background, the colour spatial distribution map fails to distinguish the salient object in the image. Figure 9 (d) demonstrates us this undesired property of colour spatial distribution, because the background is full of multiple single coloured areas that do not occur anywhere else in the image.

3.3. Learning

The three features discussed beforehand all have strengths and weaknesses in different areas, adding them together provides an accurate description of the salient area in an image. It would be over-simplistic to weight these features equally, since one feature may be better than the others at providing information about image saliency. One effective and reasonable approach to determine the optimal weights to combine the three features with is through the help of a machine learning algorithm. In this report, we implement logistic regression to decide the optimal weight on training data.

As mentioned before, the salient object detection is formulated as a binary decision problem. From this perspective, we can directly compute the posterior distribution over the binary saliency variable A_x as a sigmoid function:

$$y_x = p(A_x = 1|\boldsymbol{\phi}_x) = \frac{1}{1 + exp(-\boldsymbol{\lambda} \cdot \boldsymbol{\phi}_x)}$$

where the vector $\boldsymbol{\phi}_x$ contains three normalised energy parameters $F_k(x, I)$ for each pixel x, and the vector $\boldsymbol{\lambda} = \{\lambda_1, \lambda_2, \lambda_3\}$ indicates how the three extracted features form the unary term in the energy function are used in the inference model.

The likelihood function of an image with given human label $\boldsymbol{t}$ can be defined as such:

$$p(\boldsymbol{t}|\boldsymbol{\lambda}) = \prod_x y_x^{t_x} (1 - y_x)^{1 - t_x}$$

where the target variable $\boldsymbol{t}$ is the ground truth map, and $\boldsymbol{t}_x$ indicates the human-labelled binary saliency in the pixel x.

We apply the maxmum likelihood estimation to evaluate the parameter $\boldsymbol{\lambda}$, based on the above likelihood function. Under this logistic regression framework, the ultimately learned parameter $\boldsymbol{\lambda}$ is $(1.58137, 2.62738, 0.563939)$.

3.4. CRF Inference

The weighted unary potential made up from these weighted feature maps

$$S_{unary}(a_x, I) = \sum_{k=1}^{K} \lambda_k \cdot F_k(a_x, I)$$

is likely to already provide a good estimate of the salient area in the image. However, to capture the spatial continuity of the salient area we infer the maximum likelihood assignment of pixel-wise variables under a conditional random field (CRF) framework. A standard message-passing approach is infeasible when dealing with images at the pixel level, so we instead use α-expansion inference, which successively segments all α and non-α pixels using graph cuts [1]. The algorithm changes the value of α at each iteration using the graph cut algorithm; by this means, inferring

(a)   (b)   (c)   (d)
(a) Raw Image (b) $\lambda_0 = 1$ (c) $\lambda_0 = 10$ (d) $\lambda_0 = 100$
Figure 10. Examples for Binary Mask with various $\lambda_0 values$

(a) Raw Image (b) Combined Unary Map (c) Binary Mask ($\lambda = 10$)
Figure 11. Examples for CRF inference by α-expansion

the maximum likelihood assignment for each binary variable (or equivalently, the minimal energy function) is much faster.

This requires a way to determine the parameter λ_0 which indicates to what extent, relative to the unary potential of the combined feature map, we ought to consider the pairwise potential in deciding the binary saliency of a pixel. This parameter is key to influencing the smoothness of the resulting binary mask, since as discussed above it can be regarded as a penalty for labelling adjacent pixels with different values.

λ_0	0.1	1	10	50
Precision	0.694	0.761	0.866	0.890
Recall	0.520	0.618	0.619	0.323
F-Measure	0.589	0.659	0.704	0.399
BDE	57.09	37.78	28.56	67.96

Table 1. The table showing results of cross validaton

To determine a suitable value for λ_0, we apply cross validation at various magnitudes. It is observed that the $\lambda_0 = 10$ has relatively large F-Measure and small boundary-displacement error. Therefore, the parameter λ_0 we use for inferring the final binary mask is $\lambda_0 = 10$.

Figure 12. Examples images for bounding box output

4. Result Evaluation

The accuracy of the approach taken is shown visually in Figure 12. However, the numerical accuracy of our approach cannot be extracted from the output image. To calculate the effectiveness of our approach, we use two approaches: region-based evaluation, and boundary displacement errror.

4.1. Bounding Box

The binary mask derived from the CRF inference can be used directly in a multitude of applications. However, in order to evaluate the accuracy of our approach, we make use of OpenCV's findContours algorithm [9] to output a bounding box rectangle around the detected salient object, based on the derived pixel-wise binary mask. The dimensions of this bounding box are written to a text file holding all resultant labels for that image directory, based on which the following evaluation methods are applied to score the performance of our approach.

4.2. Evaluation Criteria

As to this project, we utilise two approaches to evaluate our result: region-based measurement and boundary-based measurement.

4.2.1 Region-based measurement

Precision and Recall both take significant roles in the information retrieval as a performance indicator. They are used in this project in evaluating the correctness of the output rectangle.

The precision represents the percentage of pixels that are correctly detected in ground truth, which is the ratio of the number of pixels in overlapped region to pixel number contained in the ground truth box. The recall reflects the percentage of pixels that are correctly detected in resulted de-

tection, which is the ratio of pixel number the overlapped region contained to the number of pixels.
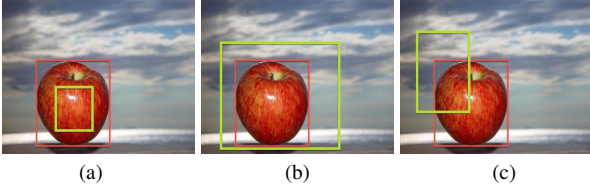

Figure 13. Examples with result and ground truth labels
Red Box: ground truth label. Green Box: detected label.

It is evident that all three results in Figure 13 are far from satisfying. The salient detection in the leftmost image has high precision but the recall is very low, meaning that it has failed to detect all truly salient pixels. The middle image is no better, with high recall but low precision, with a saliency leak into the surrounding region.

For an overall performance measurement, the F-measure indicator is suitable, with $\alpha = 0.5$ giving the weighted harmonic mean of precision and recall:

$$F_{0.5} = \frac{1.5 \times Precision \times Recall}{0.5 \times Precision + Recall}$$

where obviously puts more emphasis on precision than recall since we prefer rectangles of overly restricted size, which fails to detect thecomplete salient objects, rather than those of boxing the whole image, in which case, no saliency information is detected.

4.2.2 Boundary-based measurement

The boundary-based measurement we used is Boundary displacement error (BDE), which measures the average positional difference between the ground truth and result labels [2]. It does this by calculating the minimum Euclidian distance between the set of pixels in one label B_1 and each pixel x in the other label B_2

$$BDE(B_1, B_2) = \frac{\sum\limits_{x \in B_1} \min\limits_{y \in B_2} \{d_E(x, y)\}}{|B_1|}$$

A perfect score is 0, where every point in the result output label is contained in the set of points in the truth label. As the result labels differ more and more from the ground truth, the average BDE value becomes higher. The value itself represents the average number of pixels the result label boundaries have been displaced by as a whole, when compared to what they should be. This does not necessarily mean that the label's bounding box dimensions are proportionally the same to those of the ground truth, because smaller, larger, and offset labels can have the same boundary displacement.

4.3. Results and Discussion

The final performance evaluation is based on the test sets constructed from the MSRA dataset B. The average recall and precision in our test set is 0.629 anda 0.848 respectively. And the average harmonic measurement F-Measure is 0.705. Besides, for the boundary-based measurement, the average BDE score for our algorithm is 28.47, which means there are about 28 pixels in the **..blahblah**.

Part of the reason for this somewhat low score is that the contours around the saliency mask map are not always fully closed, leading to high precision with a bounding box rectangle around a single point of the salient area since it is the largest discovered closed surface. Creating a bounding box around all salient points in an image has the opposite effect on certain images, with a large recall but multiple non-salient areas of the image contained within the bounding box because of small areas in the image where a "saliency leak" has occurred, even after CRF inference.

5. Conclusion

In this project, we have demonstrated a supervised approach for salient object detection, formulated as a binary labelling problem using a set of local, regional, and global salient object features. However, there is much room for improvement, especially in the labelling of the salient areas from the derived binary mask. There is also a lack of comparison with other methods using numerical evaluations, which may demonstrate greater effectiveness of the approach in this report.

There are still several remaining issues for further investigation. These include the ability to detect multiple salient areas in an image, improving on previous and current work to form a computational model capable of describing a scene. Another application could be in real-time detection for use in robotics and recording or playback applications. Failure cases of the algorithm can be remedied by creating a more adept manner of finding the largest salient portion of the image, that captures the closest 98% of salient pixels. This would result in much higher numerical accuracy overall when interpreting the binary mask. There may also be better ways to derive a label from the raw binary mask of an image than finding contours or largely salient areas.

Last but not in the least, the negative effect of inherent drawback of such pixelwise learning, coming from the pseudo-correctness of ground truth data, is not removed. That is, the human-labeled rectangle may sometimes contain a large portion of pixels that are not, from the perspective of its graphic characteristics, belonging to the real salient object. For example, in the Fig.13, the ground truth label (red box) encompasses a number of blue pixels corresponding to the sky, which evidently should not be within the salient object. Such noise might be enlarged when the

brisk of true salient object is a tip. As a consequence of that, the logistic regression in this project may learn from a set of essentially erroneous pair of feature vector ϕ_x and target variable t_x and thus, the resulted parameter λ could be not precisely optimal.

References

[1] Y. Boykov, O. Veksler, and R. Zabih. Fast approximate energy minimization via graph cuts. *Pattern Analysis and Machine Intelligence, IEEE Transactions on 23.11*, pages 1222–1239, 2001. 5

[2] J. Freixenet, X. M. noz, D. Raba, J. Martí, and X. Cufí. Yet another survey on image segmentation: Region and boundary information integration. *Proc. European Conf. Computer Vision*, pages 408–422, 2002. 7

[3] S. Gould. Darwin: A framework for machine learning and computer vision research and development. *Journal of Machine Learning Research*, 13:3533–3537, 2012. 1

[4] L. Itti. Models of bottom-up and top-down visual attention. Master's thesis, California Institute of Technology Pasadena, 2000. 1

[5] L. Itti, C. Koch, and E. Niebur. A model of saliency-based visual attention for rapid scene analysis. *IEEE Transactions on Pattern Analysis and Machine Intelligence*, 20(11), November 1998. 1

[6] T. Liu, J. Sun, N.-N. Zheng, X. Tang, and H.-Y. Shum. Learning to detect a salient object. *Computer Vision and Pattern Recognition*, CVPR(7):IEEE Conference on. IEEE, 2007. 2

[7] T. Liu, Z. Yuan, J. Sun, J. Wang, N. Zheng, X. Tang, and H.-Y. Shum. Learning to detect a salient object. *Pattern Analysis and Machine Intelligence, IEEE Transactions on 33.2*, pages 353–367, 2011. 2

[8] Y.-F. Ma and H.-J. Zhang. Contrast-based image attention analysis by using fuzzy growing. *Proceedings of the eleventh ACM international conference on Multimedia. ACM*, 2003. 1

[9] S. Suzuki and K. Abe. Topological structural analysis of digitized binary images by border following. *CVGIP*, 30(1):32–46, 1985. 6